

Supplementary materials for:

Three distinct Holocene intervals of stalagmite deposition and non-deposition revealed in NW Madagascar, and their paleoclimate implications

Ny Riavo Gilbertinie Voarintsoa^{1*†}, Loren Bruce Railsback¹, George Albert Brook², Lixin Wang², Gayatri Kathayat³, Hai Cheng^{3,4}, Xianglei Li³, Richard Lawrence Edwards⁴, Amos Fety Michel Rakotondrazafy⁵, Marie Olga Madison Razanatseheny⁵

¹ Department of Geology, University of Georgia, Athens, GA 30602-2501 U.S.A.

² Department of Geography, University of Georgia, Athens, Georgia, 30602-2502 U.S.A.

³ Institute of Global Environmental Change, Xi'an Jiaotong University, Xi'an, Shaanxi 710049, P.R. China

⁴ Department of Earth Sciences, University of Minnesota, Minneapolis, Minnesota 55455, U.S.A.

⁵ Mention Sciences de la Terre et de l'Environnement, Domaine Sciences et Technologie, University d'Antananarivo, Madagascar

*Correspondence to: Ny Riavo Voarintsoa (nv1@uga.edu or nyriavony@gmail.com)

†Current address: Institute of Earth Sciences, The Hebrew University in Jerusalem, A. Safra Campus, 91904, Jerusalem, Israel (nyriavo.voarintsoa@mail.huji.ac.il)

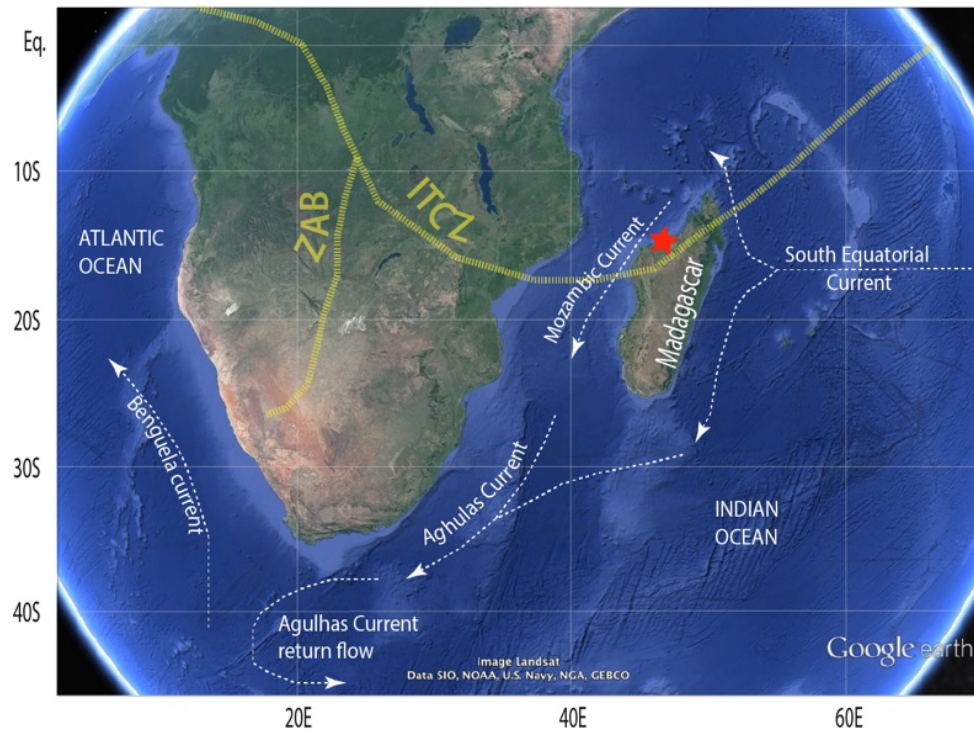


Figure S1: Google Earth image putting Madagascar into perspective with regard to oceanic currents and convergence zones (ITCZ and ZAB, Zaire Aire Boundary). The map of the currents was obtained from Lindesay (1998) and Schott and McCreary (2001). The map of the ITCZ and ZAB was adopted from Gasse (2000). The red star indicates the study location.

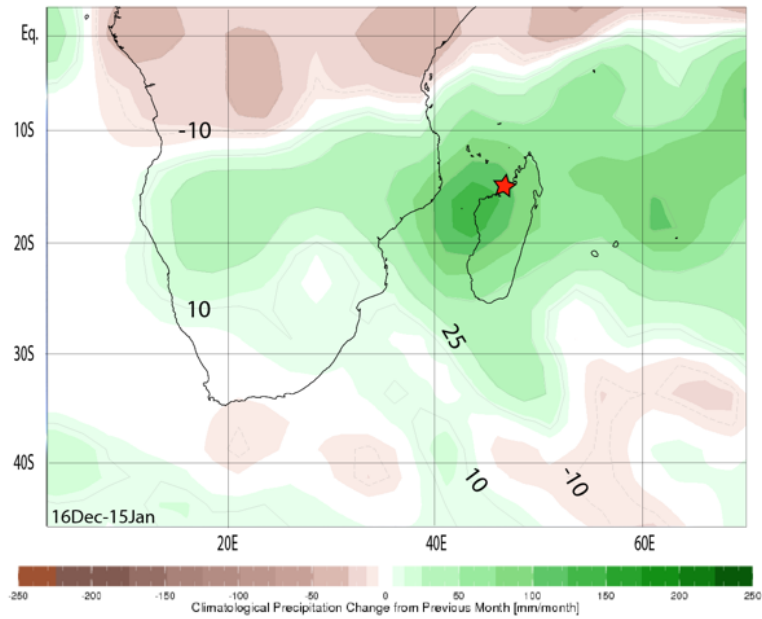
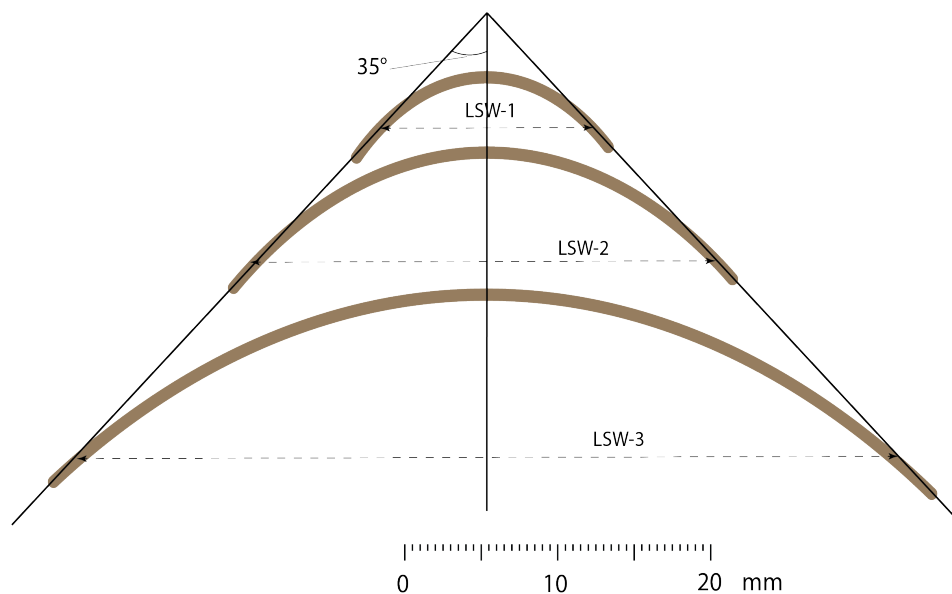


Figure S2: **Climate setting.** Map of summer precipitation between December 16 and January 15 (the wettest months) in Madagascar. Red star indicates the study area. Source: <http://iridl.ldeo.columbia.edu/> (accessed August 31, 2016)



Figure S3: **Cave locations.** Google Earth image showing the location of the two caves Anjohibe (ANJB) and Anjokipoty (ANJK) Caves and the current extent of vegetation cover in northwestern Madagascar.



41
 42 Figure S4: Scheme used to determine layer-specific width (LSW). Brown lines represent
 43 hypothetical traceable stalagmite layers.
 44

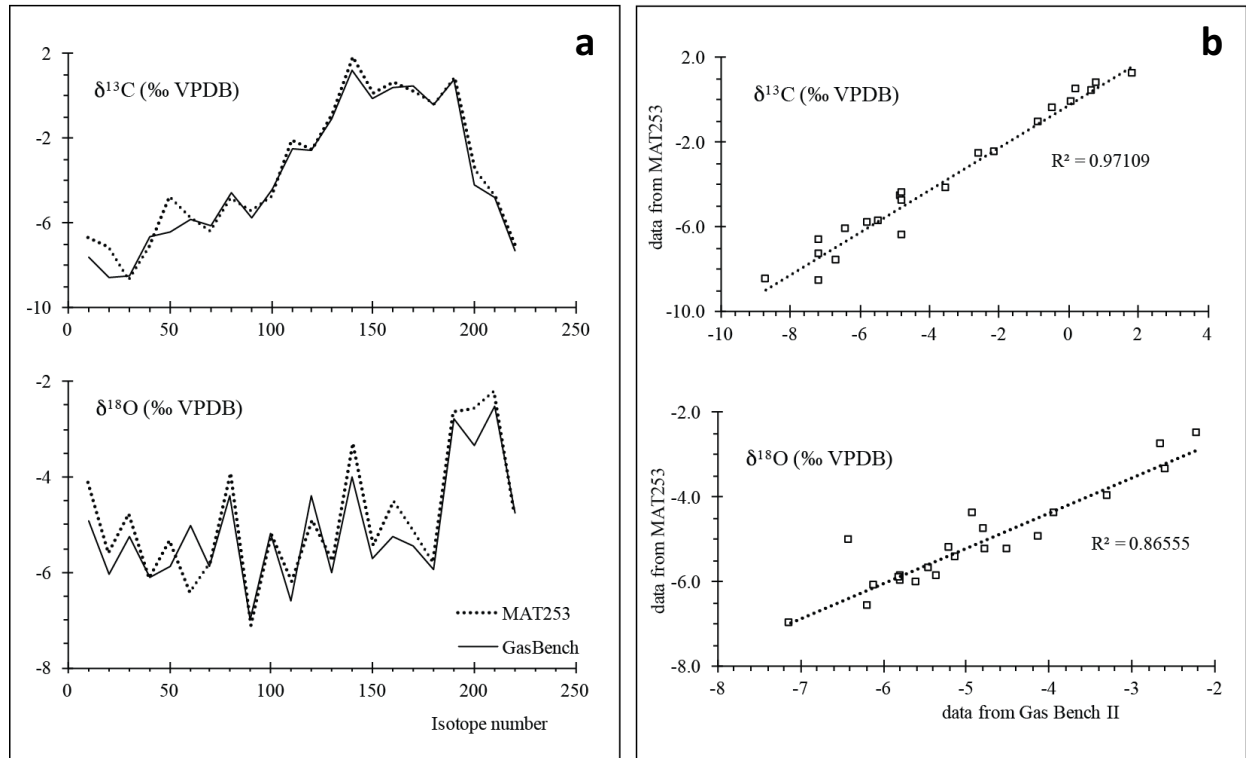


Figure S5: Comparison between MAT 253 and Gas Bench II stable isotope results on Stalagmite MAJ-5, showing similarity in the results. a) Depth series of $\delta^{13}\text{C}$ and $\delta^{18}\text{O}$. b) Scatterplots of $\delta^{13}\text{C}$ and $\delta^{18}\text{O}$.

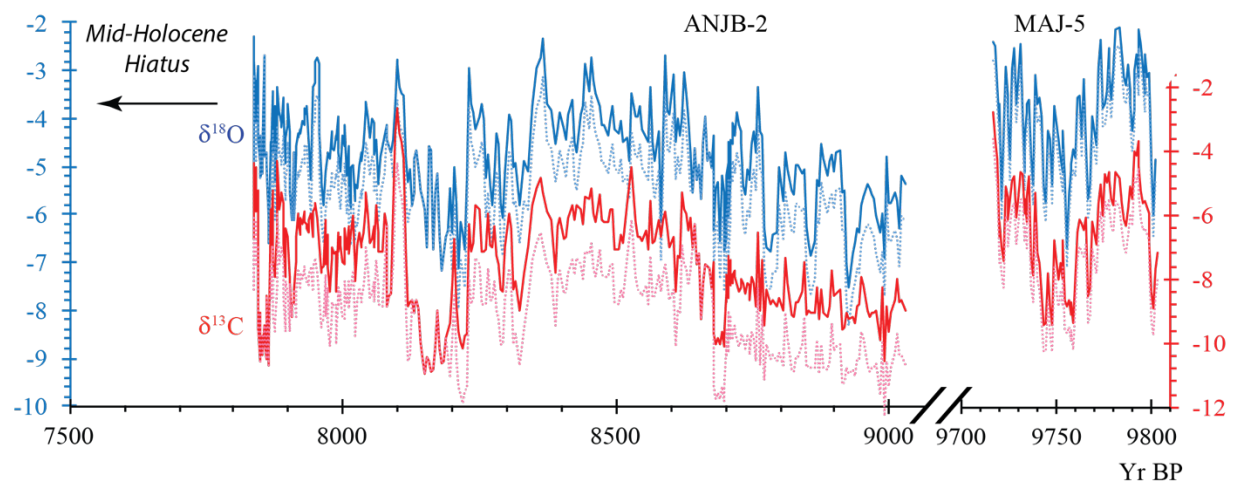


Figure S6: Profile of corrected (dashed lines) and uncorrected (continuous lines) $\delta^{18}\text{O}$ and $\delta^{13}\text{C}$ of stalagmites ANJB-2 and MAJ-5 during the MEHI.

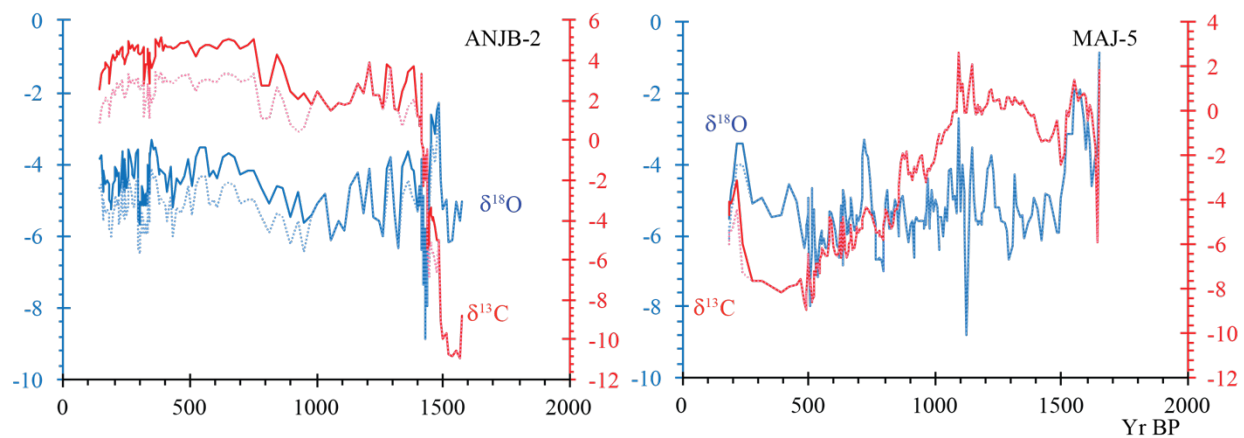


Figure S7: Profile of corrected (dashed lines) and uncorrected (continuous lines) $\delta^{18}\text{O}$ and $\delta^{13}\text{C}$ of stalagmites ANJB-2 and MAJ-5 during the MLHI.

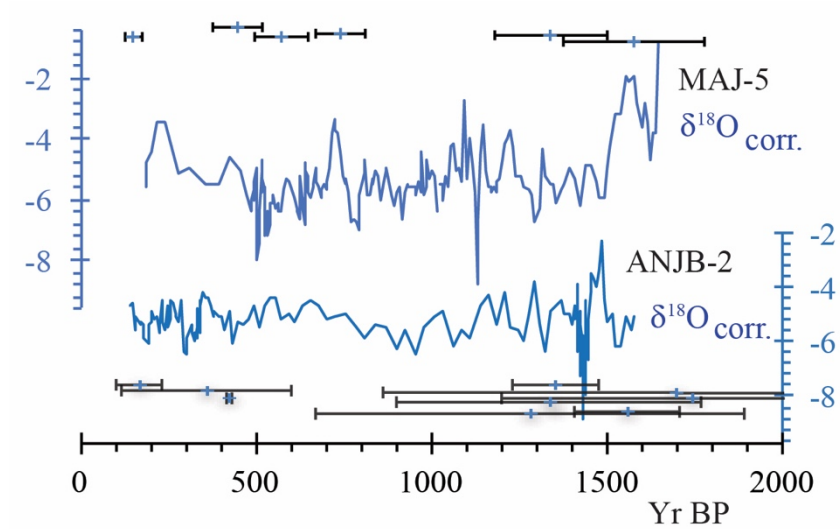


Figure S8: Comparison of the corrected $\delta^{18}\text{O}$ profiles for stalagmites MAJ-5 and ANJB-2 with their corresponding age uncertainty.

Supplementary text 1: Calcite and aragonite in stalagmites

Calcite and aragonite are two CaCO_3 polymorphs. They are the most common calcium carbonate minerals forming stalagmites. Most stalagmites are monomineralic, but bimineralic stalagmites also exist, such as the case of our stalagmites. In some cases, both minerals are primary. In some other cases, calcite replaces aragonite (e.g. Zhang et al., 2014; Lachniet et al., 2012). Of concerns of many researchers is the microscopic intermingling between calcite and aragonite (e.g. Frisia et al., 2002; Gonzalez and Lohmann, 1988; Ortega et al., 2005; Railsback et al., 1994; Woo and Choi, 2006), either as a result of diagenetic processes (e.g. Zhang et al., 2014) or purely primary crystallization of calcite and aragonite when the solution is saturated with these minerals (e.g. Sletten et al., 2013; Railsback et al., 1994). In several aragonite-bearing stalagmite, it is very likely that the aragonite-calcite mixture at microscopic level is expected (e.g. Frisia et al., 2002; Railsback et al., 1994; Lachniet et al., 2012), and this mixture, often variable in proportions (e.g. see Fig. 3 of Sletten et al., 2013; Zhang et al., 2014; Scroxton et al., 2017), could complicate interpretation of stable isotope variations (Frisia et al., 2002; Zhang et al., 2014; McMillan et al., 2005) in a strict paleoclimate context (Fairchild et al., 2006; Lachniet et al., 2012). The complication specifically arises from the different H_2O - CaCO_3 equilibrium fractionation factors for aragonite and calcite (e.g. Lachniet, 2009; Robinson and Clayton, 1969; Romanek et al., 1992; Kim et al., 2007). We were very careful with drilling and sampling to avoid mixing of the mineralogy, since layers of calcite and aragonite are distinct and sample size was very small. Investigation of the polished surface of the two stalagmites also suggests that the samples did not experience extensive diagenetic alteration, such as the case identified in Zhang et al. (2014) and Lachniet et al. (2012).

To understand the mineral distribution in our stalagmites, we run X-Ray diffraction on 15 powdered samples (Figs. S9-11), we looked at thin sections (Figs. S12, S17), and we run some SEM (Scanning Electron Microscopy) on selected intervals (Fig.S13).

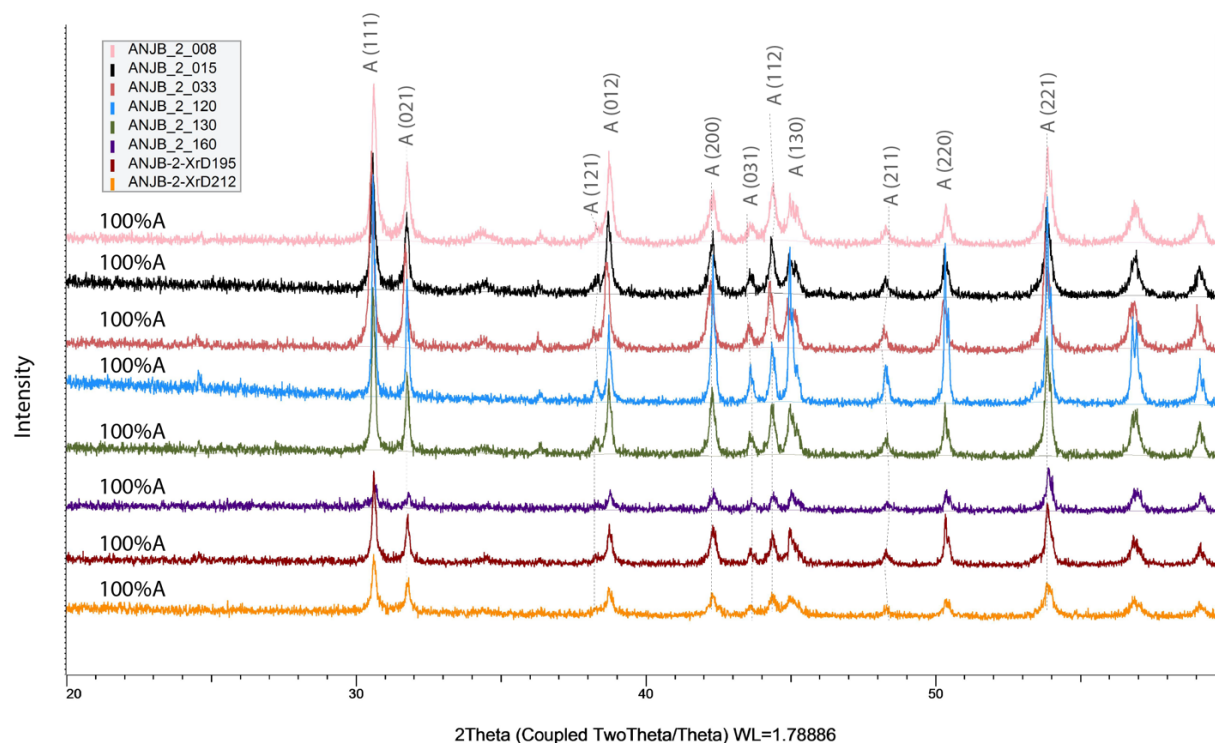


Figure S9: XRD profiles of aragonite (A) samples from different locations in Stalagmite ANJB-2. The number in parenthesis are the miller indices of the aragonite mineral.

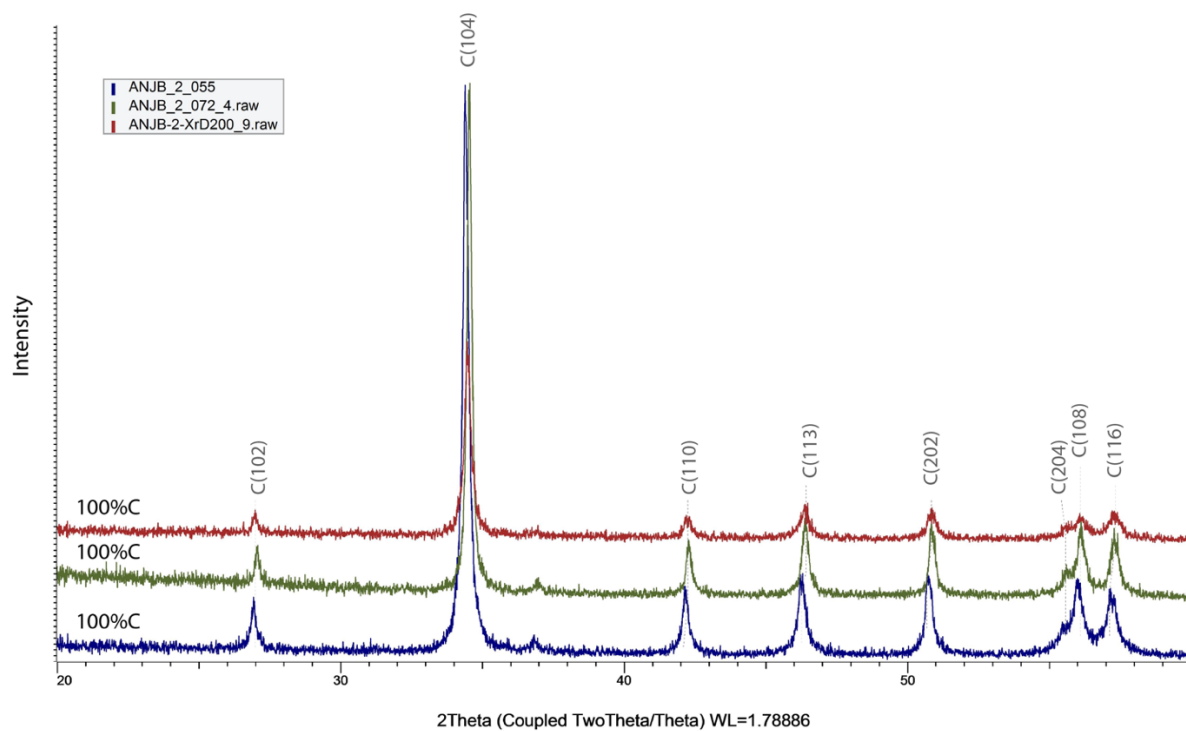


Figure S10: XRD profiles of calcite (C) samples from different locations in Stalagmite ANJB-2. The number in parenthesis are the miller indices of the aragonite mineral.

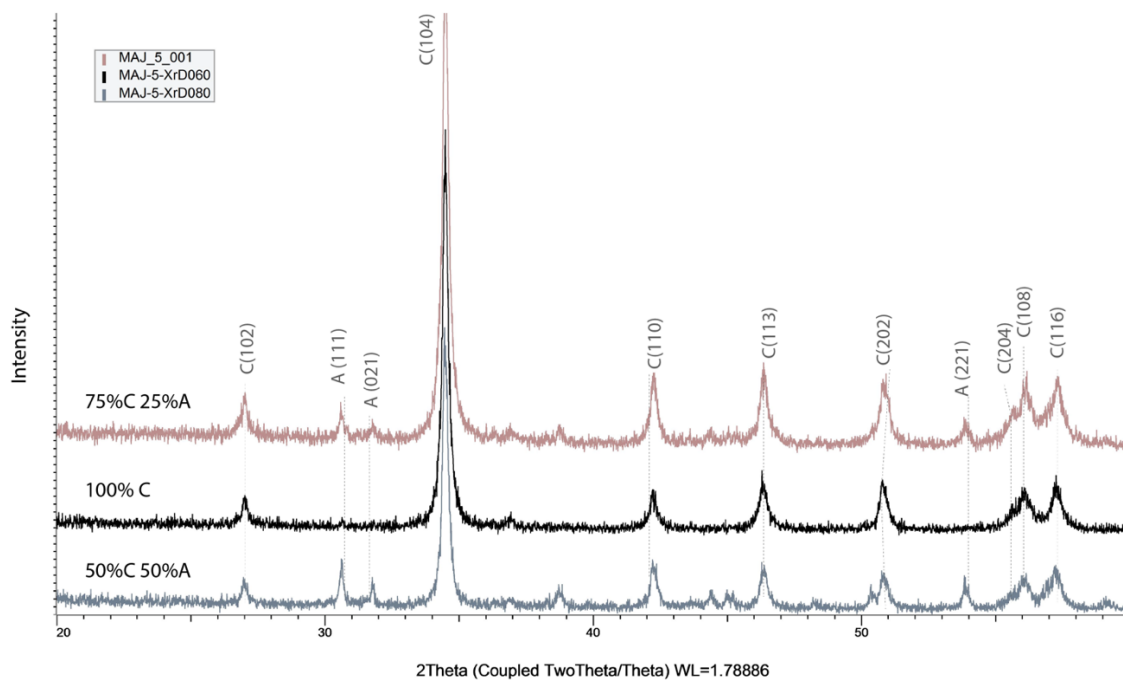


Figure S11: XRD profiles of aragonite (A) and calcite (C) samples from different locations in Stalagmite MAJ-5. The number in parenthesis are the miller indices of the mineral.

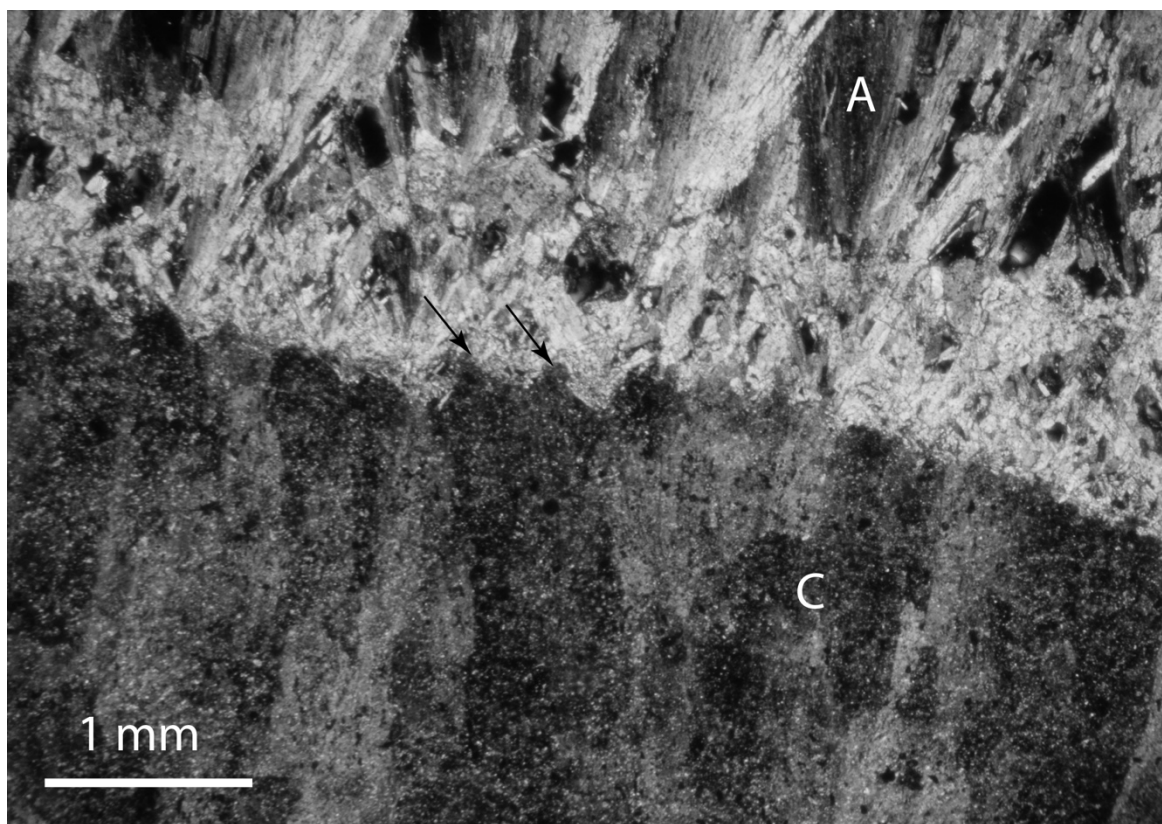


Figure S12: Microphotograph showing the sharp boundary between calcite (C) and aragonite (A) in Stalagmite ANJB-2. Indicated with two black arrows (near center of image) are two obvious pyramidal termination of calcite.

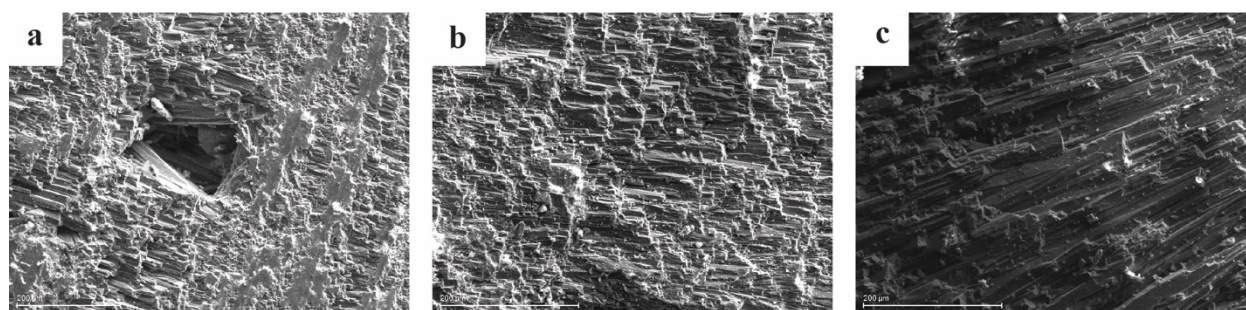


Figure S13: Scanned Electron Microscope images of a) aragonite with micro-cavities, b) columnar aragonite, and c) columnar calcite.

Supplementary text 2: Isotopic fractionation

Fractionation factors of carbon and oxygen stable isotopes between the solution and the precipitated mineral are significantly different between aragonite and calcite (Kim and O'Neil, 1997; Tarutani et al., 1969; Grosman and Ku, 1986; Kim et al., 2007; Robinson and Clayton, 1969; Turner, 1982; Romanek et al., 1992). For example, several studies have shown stable isotope enrichment in aragonite relative to calcite at similar conditions. A $\delta^{13}\text{C}$ enrichment of around 2.5‰ in the original aragonite layer from Stalagmites CL26 and CL27 (McDermott et al., 1999) was reported to approximate the theoretical expected difference between aragonite and calcite (e.g. Morse and MacKenzie, 1990). Laboratory experiments on calcium carbonate at 25°C have shown that $\delta^{13}\text{C}$ values of synthetic aragonite precipitated from a bicarbonate solution is enriched by ~1.4‰ and ~1.8‰ relative to calcite (Robinson and Clayton, 1969; Turner, 1982; Romanek et al., 1992), while $\delta^{18}\text{O}$ values is enriched by ~0.6‰ and ~0.8‰ (Tarutani et al., 1969; Kim and O'Neil, 1997; Grosman and Ku, 1986; Kim et al., 2007). Later experiments and investigations agree with these previous data (e.g. McMillan et al., 2005; Zhang et al., 2014). Some other authors have reported larger difference (16‰) between calcite $\delta^{13}\text{C}$ and aragonite $\delta^{13}\text{C}$ in speleothems (e.g. Frisia et al., 2002). We assume, based on the data presented in Frisia et al.'s (2002) specific study, that this large difference is not solely caused by aragonite's inherent fractionation of heavier isotopes at time of deposition, but also it could be associated with natural causes, such as the difference in cave environment, the degree of kinetic fractionation, and the sourcing of $\delta^{13}\text{C}$ (e.g. vegetation and biomass activity above the cave). Consequently, it would be wise to use the laboratory results from the experimental studies, i.e. the $\delta^{13}\text{C}$ value of 1.8‰ (Robinson and Clayton, 1969; Romanek et al., 1992) to correct for the differential fractionation between calcite

129 and aragonite, because the different natural variables and parameters that could alter $\delta^{13}\text{C}$ values
130 are well under control (i.e. free of other natural factors' influences).

131

132

Supplementary text 3: the 8.2 ka event in Madagascar

The 8.2 ka event has been identified in Stalagmite ANJB-2. Below are illustrative figures that show this event in the sample.

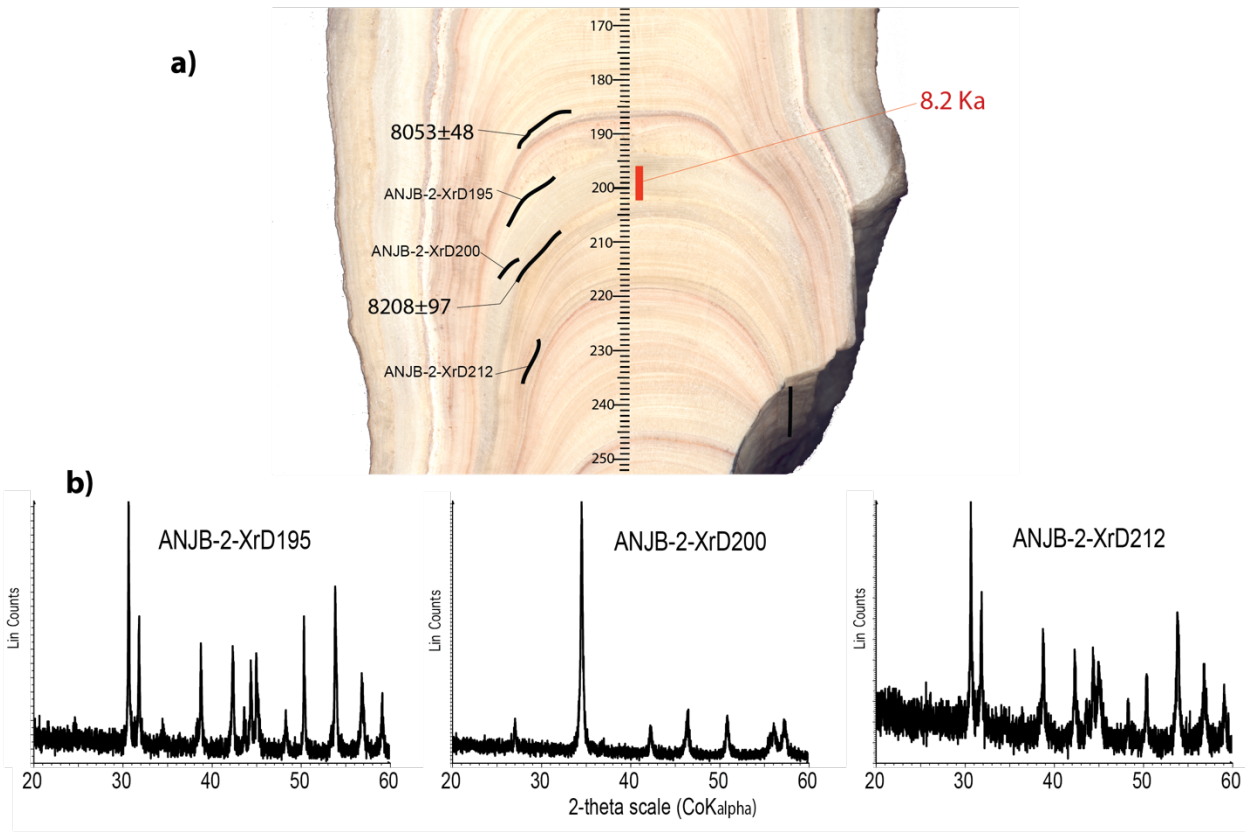
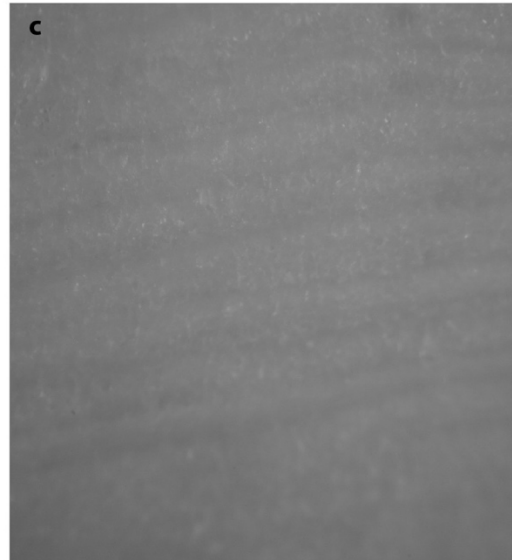
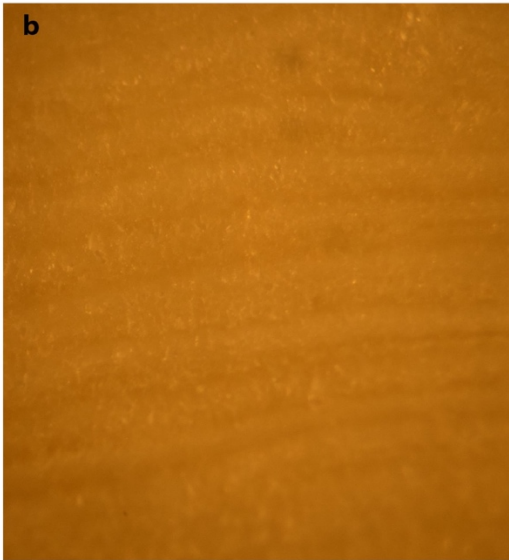
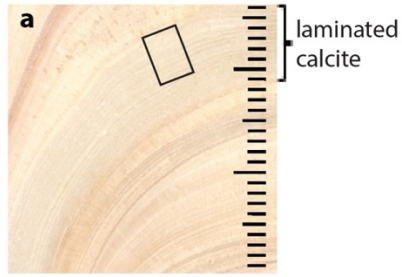


Figure S14: The 8.2 ka event identified in the Stalagmite ANJB-2 sample. a) Scanned image of a portion of Stalagmite ANJB-2 showing the 8.2 ka event and the corresponding trenches for radiometric dating (thicker black lines) and for X-ray diffraction analyses (thinner black lines). b) X-ray diffraction spectra of the stalagmite layers at 195 (aragonite), 200 (calcite), and 212 mm (aragonite) from the top of the stalagmite.

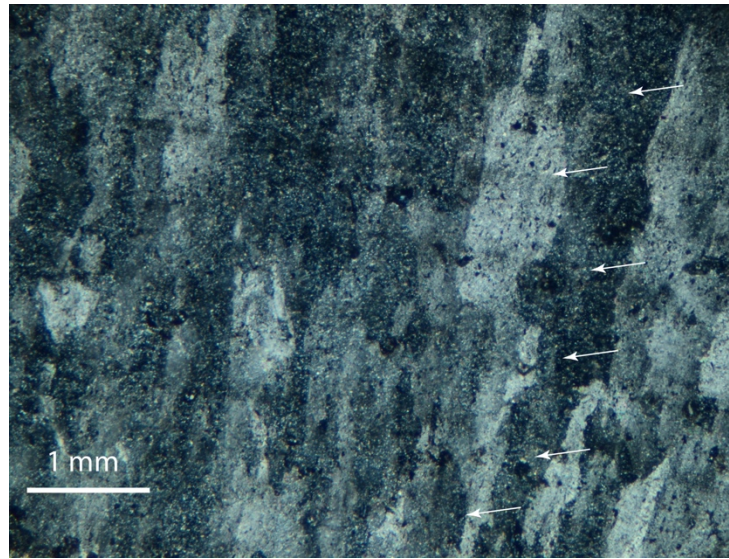


Figure S15: **Photographs illustrating the mid-Holocene hiatus.** Photographs showing the Type L layer-bounding surfaces in Stalagmite ANJB-2 (a) and in Stalagmite MAJ-5 (b). Pinching of layers toward the flank are indicated with arrows, except in Stalagmite ANJB-2 where the topmost arrow indicates aragonite. Also, note the white and porous layer of aragonite in Stalagmite ANB-2 that is capped with a very thin brown layer.



154
 155 Figure S16: Photograph showing the preserved lamination in the layer of calcite at 8.2 ka layer. (a)
 156 Scanned image of a section of Stalagmite ANJB-2 where the 8.2 was identified. (b) Photograph
 157 using true color under plain light. (c) Photograph using black and white filter.

158



159

160 Figure S17: Microphotograph of a columnar calcite with the alternating lamination revealed at the
161 8.2 ka event. Darker laminations, as seen in earlier photograph (Fig. S16), are indicated with an
162 arrow.

163

Supplementary text 4: Speculating on the IOD and ENSO influence on Madagascar climate

Although the ITCZ is the main driver of rainfall availability in Madagascar, recent studies have also suggested the importance of SST changes in the surrounding ocean and teleconnection with other climatic phenomena. Scroxton et al. (2017) linked rainfall changes in eastern Indian Ocean with expansion and contraction of the ITCZ along with positive IOD. Zinke et al. (2004) revealed strong Indian Ocean subtropical dipole events that were in phase with ENSO indices between AD 1880 and 1920, and between 1930 and 1940, and after 1970 in austral summers. Brook et al. (1999, p. 700) suggested linkages between rainfall and ENSO in NW Madagascar since AD 1550, a relationship that is less clear and complicated. This complication could be associated with an unclear or yet a limited understanding of the relationship between IOD and ENSO, which is not yet fully understood (e.g., Saji et al., 1999; Li et al., 2003; Lee et al., 2008 versus Brown et al., 2009; Schott et al., 2009; Shinoda et al., 2004; Venzke et al., 2000; Abram et al., 2008; Saji and Yagamata, 2003; Meyers et al., 2007).

Our understanding of the oceanic and atmospheric circulation is challenged because IOD and ENSO share similar features in the associated SST and precipitation anomalies (e.g., Saji et al., 1999; Webster et al., 1999; Krishnamurty and Kirtman, 2003; Meyers et al., 2007). In addition, the driving mechanisms of ENSO and IOD during the Holocene are not fully understood, even though linkages with insolation were reported (e.g., Otto-Bliesner et al., 2003; Liu et al., 2000; Timmermann et al., 2007; Zheng et al., 2008; Tudhope et al., 2001; Moy et al., 2002; Koutavas et al., 2006; Conroy et al., 2008; Kuhnert et al., 2014; Abram et al., 2007). The IOD signals in the tropical Indian Ocean may additionally be overridden by the global mean temperature (e.g., Vecchi and Soden, 2007; Zheng et al., 2013), or the signals could be strongly influenced by monsoonal changes in the surrounding landmasses (e.g., Abram et al., 2007; Qiu et al., 2012).

Despite the complicated relationships, it is possible that climate of NW Madagascar has been influenced by ITCZ, IOD, and ENSO, but this is still poorly understood during the Holocene. We are aware that the temporal and spatial resolution of available records make this investigation challenging, and we understand that the range of uncertainty of radiometric ages of several paleoclimate data could be another barrier to fully evaluate such relationship (see for example Fig. 7 of Kuhnert et al., 2014).

193 Tables

194 Table S1: ^{230}Th dating results for Stalagmite ANJB-2. The error is 2σ error. Dft= distance from the top of the stalagmite.

Dft (mm)	Sample no.	^{238}U (ppb)	^{232}Th (ppt)	$^{230}\text{Th} / ^{232}\text{Th}$ (atomic $\times 10^{-6}$)	$d^{234}\text{U}^*$ (measured)	$^{230}\text{Th} / ^{238}\text{U}$ (activity)	^{230}Th Age (yr) (uncorrected)	^{230}Th Age (yr) (corrected)	$d^{234}\text{U}_{\text{Initial}}^{**}$ (corrected)	^{230}Th Age (yr BP)*** (corrected)
3	ANJB-2-U003	3371 ±11	39850 ±809	10 ±0	5.2 ±2.0	0.0070 ±0.0001	761 ±7	419 ±243	5 ±2	355 ±243
8	ANJB-2-008	194.6 ±0.3	410 ±8	20 ±3	3.6 ±1.7	0.0026 ±0.0004	284 ±47	223 ±64	4 ±2	161 ±64
25	ANJB-2-025	4646.6 ±6.6	1594 ±32	216 ±5	3.4 ±1.4	0.0045 ±0.0001	489 ±7	479 ±10	3 ±1	417 ±10
47	ANJB-2-U047	64 ±0	634 ±15	31 ±12	3.0 ±4.3	0.0187 ±0.0074	2052 ±822	1762 ±845	3 ±4	1697 ±845
53	ANJB-2-U053R	134 ±0	2325 ±47	20 ±4	4.6 ±2.0	0.0211 ±0.0037	2313 ±416	1808 ±547	5 ±2	1743 ±547
72	ANJB-2-072	67.8 ±0.1	382 ±8	48 ±3	8.5 ±2.4	0.0163 ±0.0008	1778 ±93	1615 ±147	9 ±2	1553 ±147
92	ANJB-2-U092	78 ±0	180 ±8	92 ±40	5.1 ±3.5	0.0129 ±0.0056	1408 ±610	1341 ±612	5 ±4	1276 ±612
105	ANJB-2-U105	117 ±0	229 ±9	113 ±34	13.5 ±2.9	0.0134 ±0.0040	1450 ±432	1393 ±434	14 ±3	1329 ±434
112	ANJB-2-U112	1322 ±2	7456 ±150	42 ±2	8.5 ±2.0	0.0145 ±0.0005	1576 ±50	1413 ±125	9 ±2	1348 ±125
116	AB-1a	130.9 ±0.2	530 ±14	136.7 ±16.7	27.0 ±3.0	0.033539275 ±0.00400	3620 ±439	3506 ±446	27.2 ±3.0	3444 ±446
118	AB-2a	2569.8 ±2.9	5266 ±106	580.4 ±11.9	7.5 ±1.6	0.072126026 ±0.00032	8100 ±40	8040 ±58	7.6 ±1.6	7978 ±58
120	ANJB-2-U120	1710 ±4	20753 ±418	108 ±2	9.1 ±2.3	0.0796 ±0.0004	8955 ±48	8605 ±252	9 ±2	8541 ±252
120	ANJB-2-U120R	2075 ±3	13340 ±268	197 ±4	6.3 ±1.5	0.0767 ±0.0003	8640 ±38	8454 ±137	6 ±2	8389 ±137
130	ANJB-2-130	3042.4 ±3.8	7448 ±149	477 ±10	6.2 ±1.5	0.0709 ±0.0002	7966 ±26	7895 ±57	6 ±2	7833 ±57
160	ANJB-2-160	2994.8 ±4.1	2484 ±50	1416 ±29	4.3 ±1.5	0.0712 ±0.0002	8021 ±30	7997 ±35	4 ±2	7935 ±35
185	ANJB-2-U185	3490 ±5	6040 ±122	690 ±14	3.6 ±1.7	0.0724 ±0.0003	8167 ±33	8117 ±48	4 ±2	8053 ±48
201	ANJB-2-U205	574 ±1	1881 ±38	374 ±8	5.7 ±1.8	0.0743 ±0.0006	8367 ±70	8272 ±97	6 ±2	8208 ±97
215	ANJB-2-U215	3146 ±4	5418 ±109	713 ±15	7.0 ±1.5	0.0745 ±0.0003	8379 ±33	8329 ±48	7 ±2	8265 ±48
251	ANJB-2-U251	4246 ±5	7290 ±147	745 ±15	6.3 ±1.3	0.0776 ±0.0002	8750 ±27	8700 ±44	6 ±1	8636 ±44
275	ANJB-2-U275	6077 ±9	9132 ±184	861 ±17	4.5 ±1.5	0.0785 ±0.0002	8867 ±32	8823 ±44	5 ±2	8759 ±44
280	ANJB-2-U280	5721 ±18	5408 ±110	1360 ±28	2.4 ±1.6	0.0780 ±0.0003	8828 ±36	8801 ±41	2 ±2	8737 ±41
302	ANJB-2-U302	9833 ±44	1617 ±33	8024 ±166	5.2 ±1.9	0.0800 ±0.0004	9045 ±50	9041 ±50	5 ±2	8977 ±50

U decay constants: $\lambda_{238} = 1.55125 \times 10^{-10}$ (Jaffey et al., 1971) and $\lambda_{234} = 2.82206 \times 10^{-6}$ (Cheng et al., 2013). Th decay constant: $\lambda_{230} = 9.1705 \times 10^{-6}$ (Cheng et al., 2013).

* $\delta^{234}\text{U} = ([^{234}\text{U}/^{238}\text{U}]_{\text{activity}} - 1) \times 1000$. ** $\delta^{234}\text{U}_{\text{initial}}$ was calculated based on ^{230}Th age (T), i.e., $\delta^{234}\text{U}_{\text{initial}} = \delta^{234}\text{U}_{\text{measured}} \times e^{\lambda_{234}T}$.

Corrected ^{230}Th ages assume the initial $^{230}\text{Th}/^{232}\text{Th}$ atomic ratio of $4.4 \pm 2.2 \times 10^{-6}$. Those are the values for a material at secular equilibrium, with the bulk earth $^{232}\text{Th}/^{238}\text{U}$ value of 3.8. The errors are arbitrarily assumed to be 50%.

***B.P. stands for “Before Present” where the “Present” is defined as the year 1950 A.D.

Table S2: ^{230}Th dating results for Stalagmite MAJ-5. The error is 2 σ error. Dft= distance from the top of the stalagmite.

Dft (mm)	Sample no.	^{238}U (ppb)	^{232}Th (ppt)	$^{230}\text{Th}/^{232}\text{Th}$ (atomic $\times 10^{-6}$)	$d^{234}\text{U}^*$ (measured)	$^{230}\text{Th}/^{238}\text{U}$ (activity)	^{230}Th Age (yr) (uncorrected)	^{230}Th Age (yr) (corrected)	$d^{234}\text{U}_{\text{initial}}^{**}$ (corrected)	^{230}Th Age (yr BP)*** (corrected)
1	MAJ-5-U001	2734 ± 15	3044 ± 63	33 ± 1	-3.2 ± 2.7	0.0023 ± 0.0000	246 ± 5	214 ± 24	-3 ± 3	150 ± 24
10	MAJ-5-U010	6691 ± 38	22757 ± 474	27 ± 1	-3.1 ± 3.6	0.0056 ± 0.0001	609 ± 7	510 ± 71	-3 ± 4	446 ± 71
22	MAJ-5-U022	3292 ± 4	11633 ± 234	31 ± 1	-3.0 ± 1.5	0.0067 ± 0.0001	736 ± 14	633 ± 74	-3 ± 1	569 ± 74
41	MAJ-5-U041	1380 ± 3	10604 ± 213	32 ± 1	-1.1 ± 2.1	0.0147 ± 0.0001	1617 ± 15	1393 ± 159	-1 ± 2	1329 ± 159
50	MAJ-5-U050	1224 ± 4	4144 ± 84	40 ± 1	-2.9 ± 2.4	0.0082 ± 0.0001	898 ± 15	799 ± 71	-3 ± 2	735 ± 71
60	MAJ-5-U060	1578 ± 3	14591 ± 293	31 ± 1	-0.9 ± 2.6	0.0173 ± 0.0005	1901 ± 56	1631 ± 199	-1 ± 3	1567 ± 199
66	MAJ-5-U066	12609 ± 83	38990 ± 842	461 ± 10	-4.6 ± 2.9	0.0865 ± 0.0006	9912 ± 81	9821 ± 103	-5 ± 3	9757 ± 103
80	MAJ-5-U080	11684 ± 16	27838 ± 559	598 ± 12	-2.6 ± 1.2	0.0864 ± 0.0002	9882 ± 24	9813 ± 55	-3 ± 1	9749 ± 55
89	MAJ-5-U089	10930 ± 12	30247 ± 606	519 ± 10	-1.2 ± 1.3	0.0870 ± 0.0002	9941 ± 29	9860 ± 64	-1 ± 1	9796 ± 64

U decay constants: $\lambda_{238} = 1.55125 \times 10^{-10}$ (Jaffey et al., 1971) and $\lambda_{234} = 2.82206 \times 10^{-6}$ (Cheng et al., 2013). Th decay constant: $\lambda_{230} = 9.1705 \times 10^{-6}$ (Cheng et al., 2013).

* $\delta^{234}\text{U} = ([^{234}\text{U}/^{238}\text{U}]_{\text{activity}} - 1) \times 1000$. ** $\delta^{234}\text{U}_{\text{initial}}$ was calculated based on ^{230}Th age (T), i.e., $\delta^{234}\text{U}_{\text{initial}} = \delta^{234}\text{U}_{\text{measured}} \times e^{\lambda_{234}T}$.

Corrected ^{230}Th ages assume the initial $^{230}\text{Th}/^{232}\text{Th}$ atomic ratio of $4.4 \pm 2.2 \times 10^{-6}$. Those are the values for a material at secular equilibrium, with the bulk earth $^{232}\text{Th}/^{238}\text{U}$ value of 3.8. The errors are arbitrarily assumed to be 50%.

***B.P. stands for “Before Present” where the “Present” is defined as the year 1950 A.D.

211 Table S3: Summary of the Holocene climate variability in SE Africa and SW Indian Ocean. The Holocene subdivision is relative to the
 212 MEHI, MMHI, and MLHI. “w” indicates “wet” (more rainfall) and “d” indicates “dry” (less rainfall). Please note that these inferences are
 213 relative and the temporal resolution of the sediment records are generally coarser than our stalagmite records. The most relevant
 214 paleoclimate records to NW Madagascar hitherto are indicated in stars (*)
 215

Location	Time range	Lat.	Long.	Proxy	Holocene			References
					early	middle	late	
Lake Challa (a crater lake on the lower east slope of Mt Kilimanjaro)	0-25ka	3°19'S	37°42'E	BIT index from lake deposits	w	d	w	Verschuren et al., 2009
Lake Tanganyika NP04-KH04-3A-1K and NP04-KH04-4A-1K	0-60ka	6°42'S	29°50'E	TEX ₈₆ and δD_{leaf} wax (‰ vs. SMOW)	w	w/d	d	Tierney et al., 2008
Lake Masoko	0-45ka	9°20.0'S	33°45.3'E	Low field magnetic susceptibility	w/d	d	w	Garcin et al., 2006
Lake Malawi	0-140ka	10°01.06'S 11°17.66'S	34°11.16'E 34°26.15'E	C ₂₈ δD (‰ vs. SMOW)	d/w	d	w	Konecky et al., 2011
Lake Malawi M98-1P	0-25ka	10°15.9'S	34°19.1'E	BSi MAR	w	w	d	Johnson et al. 2002
Lake Malawi M98-2P	0-25ka	9°58.6'S	34°13.8'E	BSi MAR	d	d/w	d/w	Johnson et al. 2002
*Zambezi delta (GeoB9307-3)	0-17ka (130y resolution)	18°33.9'S	37°22.8'E	δD <i>n</i> -C ₃₁ alkane (‰ vs. SMOW)	w	d	w	Schefuß et al., 2011

*Indian Ocean (MD79257)	0-45ka	20°24'S	36°20'E	Alkenone SST record	26.5°	27.25°	27°	Bard et al., 1997; Sonzogni et al., 1998
Wonderkrater	0-20ka	24.4390°S	28.7507°E	Pollen	<i>w</i>	<i>w</i>	<i>d/w</i>	Truc et al., 2013 (note some discrepancies in interpretation with Scott and Thackeray, 1987; and Scott, 1999)
Tswaing Crater	0-200ka	25°24'29.26"S	28° 4'57.32"E	Sediment composition	<i>d</i>	<i>d/w</i>	<i>w</i>	(Partridge et al., 1997)
Lake Chilwa	0-44ka	15°30'S	35°30'E	OSL dating of sediment cores	<i>w</i>	<i>d</i>	<i>d</i>	Thomas et al., 2009
Cold Air Cave	0-25ka	24°1'S	29°11'E	Stalagmite T8	<i>w</i>	<i>d</i>	<i>d</i>	Lee-Thorp et al., 2001; Holmgren et al., 2003
*Lake Tritrivakely	0-40ka	19°47'S	46°55'E	Sediment magnetic properties and pollen	<i>d</i>	<i>d/w</i>	<i>w/d</i>	Gasse et al., 1994; Williamson et al., 1998; Gasse and Van Campo, 1998
*Anjohibe Cave	1-9ka	15.53°S	46.88°E	Stalagmite	<i>w</i>	<i>d</i>	<i>d?</i>	Wang and Brook., 2013; Wang, 2016

216

217

218 **References**

- 219 Abram, N. J., Gagan, M. K., Cole, J. E., Hantoro, W. S., and Mudelsee, M.: Recent intensification of
220 tropical climate variability in the Indian Ocean, *Nature Geosci*, 1, 849-853, 2008.
- 221 Abram, N. J., Gagan, M. K., Liu, Z. Y., Hantoro, W. S., McCulloch, M. T., and Suwargadi, B. W.:
222 Seasonal characteristics of the Indian Ocean Dipole during the Holocene epoch, *Nature*,
223 445, 299-302, Doi 10.1038/Nature05477, 2007.
- 224 Bard, E., Rostek, F., and Sonzogni, C.: Interhemispheric synchrony of the last deglaciation inferred
225 from alkenone palaeothermometry, *Nature*, 385, 707-710, Doi 10.1038/385707a0, 1997.
- 226 Brook, G. A., Rafter, M. A., Railsback, L. B., Sheen, S. W., and Lundberg, J.: A high-resolution proxy
227 record of rainfall and ENSO since AD 1550 from layering in stalagmites from Anjohibe Cave,
228 Madagascar, *Holocene*, 9, 695-705, Doi 10.1191/095968399677907790, 1999.
- 229 Brown, J., Lynch, A. H., and Marshall, A. G.: Variability of the Indian Ocean Dipole in coupled model
230 paleoclimate simulations, *J Geophys Res-Atmos*, 114, 10.1029/2008jd010346, 2009.
- 231 Cheng, H., Edwards, R. L., Shen, C. C., Polyak, V. J., Asmerom, Y., Woodhead, J., Hellstrom, J., Wang,
232 Y. J., Kong, X. G., Spotl, C., Wang, X. F., and Alexander, E. C.: Improvements in Th-230 dating,
233 Th-230 and U-234 half-life values, and U-Th isotopic measurements by multi-collector
234 inductively coupled plasma mass spectrometry, *Earth Planet Sc Lett*, 371, 82-91, Doi
235 10.1016/J.Epsl.2013.04.006, 2013.
- 236 Conroy, J. L., Overpeck, J. T., Cole, J. E., Shanahan, T. M., and Steinitz-Kannan, M.: Holocene
237 changes in eastern tropical Pacific climate inferred from a Galápagos lake sediment record,
238 *Quaternary Sci Rev*, 27, 1166-1180, 2008.

239 Fairchild, I. J., Smith, C. L., Baker, A., Fuller, L., Spötl, C., Matthey, D., McDermott, F., and E.I.M.F.:
 240 Modification and preservation of environmental signals in speleothems, *Earth-Sci Rev*, 75,
 241 105-153, <http://dx.doi.org/10.1016/j.earscirev.2005.08.003>, 2006.

242 Frisia, S., Borsato, A., Fairchild, I. J., McDermott, F., and Selmo, E. M.: Aragonite–calcite
 243 relationships in speleothems (Grotte de Clamouse, France): environment, fabrics, and
 244 carbonate geochemistry., *J Sediment Res*, 772, 687-699, 2002.

245 Garcin, Y., Vincens, A., Williamson, D., Guiot, J., and Buchet, G.: Wet phases in tropical southern
 246 Africa during the last glacial period, *Geophys Res Lett*, 33, 10.1029/2005GL025531, 2006.

247 Gasse, F., Cortijo, E., Disnar, J.R., Ferry, L., Gibert, E., Kissel, C., Laggoun-Defarge, F., Lallier-Verges,
 248 E., Miskovsky, J.C., Ratsimbazafy, B., Ranaivo, F., Tucholka, P., Saos, J.L., Siffedine, A., Taieb,
 249 M., Van Campo, E., Williamson, D.: A 36 kyr environmental record in the southern tropics:
 250 Lake Tritrivakely, *Comptes-Rendus de l'Académie des Sciences, Paris, série II* 318, 1513-
 251 1519, 1994.

252 Gasse, F., and Van Campo, E.: A 40,000-yr pollen and diatom record from Lake Tritrivakely,
 253 Madagascar, in the southern tropics, *Quaternary Res*, 49, 299-311, Doi
 254 10.1006/Qres.1998.1967, 1998.

255 Gasse, F.: Hydrological changes in the African tropics since the Last Glacial Maximum, *Quaternary*
 256 *Sci Rev*, 19, 189-211, Doi 10.1016/S0277-3791(99)00061-X, 2000.

257 Gonzalez, L. A., and Lohmann, K. C.: Controls on Mineralogy and Composition of Spelean
 258 Carbonates: Carlsbad Caverns, New Mexico, in: *Paleokarst*, edited by: James, N. P., and
 259 Choquette, P. W., Springer New York, New York, NY, 81-101, 1988.

260 Grossman, E. L., and Ku, T.-L.: Oxygen and carbon isotope fractionation in biogenic aragonite:
 261 Temperature effects, Chemical Geology: Isotope Geoscience section, 59, 59-74,
 262 [http://dx.doi.org/10.1016/0168-9622\(86\)90057-6](http://dx.doi.org/10.1016/0168-9622(86)90057-6), 1986.

263 Holmgren, K., Lee-Thorp, J. A., Cooper, G. R. J., Lundblad, K., Partridge, T. C., Scott, L., Sithaldeen,
 264 R., Talma, A. S., and Tyson, P. D.: Persistent millennial-scale climatic variability over the past
 265 25,000 years in Southern Africa, Quaternary Sci Rev, 22, 2311-2326, 10.1016/S0277-
 266 3791(03)00204-X, 2003.

267 Jaffey, A. H., Flynn, K. F., Glendenin, L. E., Bentley, W. C., and Essling, A. M.: Precision measurement
 268 of half-lives and specific activities of U-235 and U-238, Phys Rev C, 4, 1889-1906, DOI
 269 10.1103/PhysRevC.4.1889, 1971.

270 Johnson, T.C.: Biogenic Silica Profiles in the Sediments of Large Tropical Lakes: Examples from East
 271 Africa, in: Sedimentation in Continental Rifts, pp. 247-255, 2002.

272 Kim, S. T., O'Neil, J. R., Hillaire-Marcel, C., and Mucci, A.: Oxygen isotope fractionation between
 273 synthetic aragonite and water: Influence of temperature and Mg²⁺ concentration,
 274 Geochim Cosmochim Ac, 71, 4704-4715, 10.1016/J.Gca.2007.04.019, 2007.

275 Kim, S.-T., and O'Neil, J. R.: Equilibrium and nonequilibrium oxygen isotope effects in synthetic
 276 carbonates, Geochim Cosmochim Ac, 61, 3461-3475, doi.org/10.1016/S0016-
 277 7037(97)00169-5, 1997.

278 Konecky, B. L., Russell, J. M., Johnson, T. C., Brown, E. T., Berke, M. A., Werne, J. P., and Huang, Y.
 279 S.: Atmospheric circulation patterns during late Pleistocene climate changes at Lake
 280 Malawi, Africa, Earth Planet Sc Lett, 312, 318-326, 10.1016/j.epsl.2011.10.020, 2011.

281 Koutavas, A., deMenocal, P. B., Olive, G. C., and Lynch-Stieglitz, J.: Mid-Holocene El Niño–Southern
 282 Oscillation (ENSO) attenuation revealed by individual foraminifera in eastern tropical
 283 Pacific sediments, *Geology*, 34, 993-996, 10.1130/G22810A.1, 2006.

284 Krishnamurthy, V., and Kirtman, B. P.: Variability of the Indian Ocean: Relation to monsoon and
 285 ENSO, *Q J Roy Meteor Soc*, 129, 1623-1646, 10.1256/qj.01.166, 2003.

286 Kuhnert, H., Kuhlmann, H., Mohtadi, M., Meggers, H., Baumann, K. H., and Patzold, J.: Holocene
 287 tropical western Indian Ocean sea surface temperatures in covariation with climatic
 288 changes in the Indonesian region, *Paleoceanography*, 29, 423-437,
 289 10.1002/2013pa002555, 2014.

290 Lachniet, M. S.: Climatic and environmental controls on speleothem oxygen-isotope values,
 291 *Quaternary Sci Rev*, 28, 412-432, Doi 10.1016/J.Quascirev.2008.10.021, 2009.

292 Lachniet, M. S., Bernal, J. P., Asmerom, Y., and Polyak, V.: Uranium loss and aragonite-calcite age
 293 discordance in a calcitized aragonite stalagmite, *Quat Geochronol*, 14, 26-37,
 294 10.1016/j.quageo.2012.08.003, 2012.

295 Lee, T., and McPhaden, M. J.: Decadal phase change in large-scale sea level and winds in the Indo-
 296 Pacific region at the end of the 20th century, *Geophys Res Lett*, 35,
 297 10.1029/2007gl032419, 2008.

298 Lee-Thorp, J. A., Holmgren, K., Lauritzen, S. E., Linge, H., Moberg, A., Partridge, T. C., Stevenson,
 299 C., and Tyson, P. D.: Rapid climate shifts in the southern African interior throughout the
 300 Mid to Late Holocene, *Geophys Res Lett*, 28, 4507-4510, 10.1029/2000GL012728, 2001.

301 Li, T., Wang, B., Chang, C. P., and Zhang, Y. S.: A theory for the Indian Ocean dipole-zonal mode, *J*
 302 *Atmos Sci*, 60, 2119-2135, 10.1175/1520-0469(2003)060<2119:Atftio>2.0.Co;2, 2003.

303 Lindesay, J. A.: Present Climates of Southern Africa, in: Climates of the Southern Continents:
 304 Present, Past and Future, edited by: Hobbs, J. E., Lindesay, J. A., and Bridgman, H. A., John
 305 Wiley & Sons Ltd., England, 5-62, 1998.

306 Liu, Z., Kutzbach, J., and Wu, L.: Modeling climate shift of El Nino variability in the Holocene,
 307 Geophys Res Lett, 27, 2265-2268, 10.1029/2000GL011452, 2000.

308 McDermott, F., Frisia, S., Huang, Y., Longinelli, A., Spiro, B., Heaton, T. H. E., Hawkesworth, C. J.,
 309 Borsato, A., Keppens, E., Fairchild, I. J., van der Borg, K., Verheyden, S., and Selmo, E.:
 310 Holocene climate variability in Europe: Evidence from $\delta^{18}\text{O}$, textural and extension-rate
 311 variations in three speleothems, Quaternary Sci Rev, 18, 1021-1038,
 312 [http://dx.doi.org/10.1016/S0277-3791\(98\)00107-3](http://dx.doi.org/10.1016/S0277-3791(98)00107-3), 1999.

313 McMillan, E. A., Fairchild, I. J., Frisia, S., Borsato, A., and McDermott, F.: Annual trace element
 314 cycles in calcite-aragonite speleothems: evidence of drought in the western
 315 Mediterranean 1200-1100 yr BP, J Quaternary Sci, 20, 423-433, 10.1002/jqs.943, 2005.

316 Meyers, G., McIntosh, P., Pigot, L., and Pook, M.: The Years of El Niño, La Niña, and Interactions
 317 with the Tropical Indian Ocean, J Climate, 20, 2872-2880, 10.1175/JCLI4152.1, 2007.

318 Morse, J.W., and Mackenzie, F.T.: Geochemistry of Sedimentary Carbonates: Amsterdam Elsevier,
 319 707 pp, 1990.

320 Moy, C. M., Seltzer, G. O., Rodbell, D. T., and Anderson, D. M.: Variability of El Nino/Southern
 321 Oscillation activity at millennial timescales during the Holocene epoch, Nature, 420, 162-
 322 165, 2002.

323 Ortega, R., Maire, R., Devès, G., and Quinif, Y.: High-resolution mapping of uranium and other trace
 324 elements in recrystallized aragonite–calcite speleothems from caves in the Pyrenees

325 (France): Implication for U-series dating, *Earth Planet Sc Lett*, 237, 911-923,
 326 <http://dx.doi.org/10.1016/j.epsl.2005.06.045>, 2005.

327 Otto-Bliesner, B. L., Brady, E. C., Shin, S.-I., Liu, Z., and Shields, C.: Modeling El Niño and its tropical
 328 teleconnections during the last glacial-interglacial cycle, *Geophys Res Lett*, 30, n/a-n/a,
 329 [10.1029/2003GL018553](http://dx.doi.org/10.1029/2003GL018553), 2003.

330 Partridge, T. C., Demenocal, P. B., Lorentz, S. A., Paiker, M. J., and Vogel, J. C.: Orbital forcing of
 331 climate over South Africa: A 200,000-year rainfall record from the Pretoria saltpan,
 332 *Quaternary Sci Rev*, 16, 1125-1133, 1997.

333 Qiu, Y., Cai, W., Li, L., and Guo, X.: Argo profiles variability of barrier layer in the tropical Indian
 334 Ocean and its relationship with the Indian Ocean Dipole, *Geophys Res Lett*, 39, n/a-n/a,
 335 [10.1029/2012GL051441](http://dx.doi.org/10.1029/2012GL051441), 2012.

336 Railsback, L. B., Brook, G. A., Chen, J., Kalin, R., and Fleisher, C. J.: Environmental Controls on the
 337 Petrology of a Late Holocene Speleothem from Botswana with annual layers of aragonite
 338 and calcite, *J Sediment Res A*, 64, 147-155, 1994.

339 Romanek, C. S., Grossman, E. L., and Morse, J. W.: Carbon Isotopic Fractionation in Synthetic
 340 Aragonite and Calcite - Effects of Temperature and Precipitation Rate, *Geochim
 341 Cosmochim Ac*, 56, 419-430, [Doi 10.1016/0016-7037\(92\)90142-6](http://dx.doi.org/10.1016/0016-7037(92)90142-6), 1992.

342 Robinson, M., and Clayton, R. N.: Carbon-13 fractionation between aragonite and calcite, *Geochim
 343 Cosmochim Ac*, 33, 997-1002, 1969.

344 Saji, N. H., and Yamagata, T.: Possible impacts of Indian Ocean Dipole mode events on global
 345 climate, *Clim Res*, 25, 151-169, [Doi 10.3354/Cr025151](http://dx.doi.org/10.3354/Cr025151), 2003.

346 Saji, N. H., Goswami, B. N., Vinayachandran, P. N., and Yamagata, T.: A dipole mode in the tropical
 347 Indian Ocean, *Nature*, 401, 360-363, 10.1038/43855, 1999.

348 Schefuß, E., Kuhlmann, H., Mollenhauer, G., Prange, M., and Patzold, J.: Forcing of wet phases in
 349 southeast Africa over the past 17,000 years, *Nature*, 480, 509-512, DOI
 350 10.1038/nature10685, 2011.

351 Schott, F. A., and McCreary, J. P.: The monsoon circulation of the Indian Ocean, *Prog Oceanogr*,
 352 51, 1-123, Doi 10.1016/S0079-6611(01)00083-0, 2001.

353 Schott, F. A., Xie, S. P., and McCreary, J. P.: Indian Ocean Circulation and Climate Variability, *Rev*
 354 *Geophys*, 47, 10.1029/2007rg000245, 2009.

355 Scott, L.: Vegetation history and climate in the Savanna biome South Africa since 190,000 ka: a
 356 comparison of pollen data from the Tswaing Crater (the Pretoria Saltpan) and
 357 Wonderkrater, *Quatern Int*, 57, 215-223, 1999.

358 Scott, L., Thackeray, J.F.: Multivariate analysis of Late Pleistocene and Holocene pollen spectra
 359 from Wonderkrater, Transvaal, South Africa. *S Afr J Sci*, 83, 93–98. 1987.

360 Scropton, N., Burns, S. J., McGee, D., Hardt, B., Godfrey, L. R., Ranivoharimanana, L., and Faina, P.:
 361 Hemispherically in-phase precipitation variability over the last 1700 years in a Madagascar
 362 speleothem record, *Quaternary Sci Rev*, 164, 25-36, 10.1016/j.quascirev.2017.03.017,
 363 2017.

364 Shinoda, T., Alexander, M. A., and Hendon, H. H.: Remote Response of the Indian Ocean to
 365 Interannual SST Variations in the Tropical Pacific, *J Climate*, 17, 362-372, 10.1175/1520-
 366 0442(2004)017<0362:RROTIO>2.0.CO;2, 2004.

367 Sletten, H. R., Railsback, L. B., Liang, F. Y., Brook, G. A., Marais, E., Hardt, B. F., Cheng, H., and
 368 Edwards, R. L.: A petrographic and geochemical record of climate change over the last 4600
 369 years from a northern Namibia stalagmite, with evidence of abruptly wetter climate at the
 370 beginning of southern Africa's Iron Age, *Palaeogeogr Palaeocl*, 376, 149-162, Doi
 371 10.1016/J.Palaeo.2013.02.030, 2013.

372 Sonzogni, C., Bard, E., and Rostek, F.: Tropical sea-surface temperatures during the last glacial
 373 period: a view based on alkenones in Indian Ocean sediments, *Quaternary Sci Rev*, 17,
 374 1185-1201, [http://dx.doi.org/10.1016/S0277-3791\(97\)00099-1](http://dx.doi.org/10.1016/S0277-3791(97)00099-1), 1998.

375 Tarutani, T., Clayton, R. N., and Mayeda, T. K.: The effect of polymorphism and magnesium
 376 substitution on oxygen isotope fractionation between calcium carbonate and water,
 377 *Geochim Cosmochim Ac*, 33, 987-996, [http://dx.doi.org/10.1016/0016-7037\(69\)90108-2](http://dx.doi.org/10.1016/0016-7037(69)90108-2),
 378 1969.

379 Thomas, D. S. G., Bailey, R., Shaw, P. A., Durcan, J. A., and Singarayer, J. S.: Late Quaternary
 380 highstands at Lake Chilwa, Malawi: Frequency, timing and possible forcing mechanisms in
 381 the last 44ka, *Quaternary Sci Rev*, 28, 526-539,
 382 <http://dx.doi.org/10.1016/j.quascirev.2008.10.023>, 2009.

383 Tierney, J. E., Russell, J. M., Huang, Y., Damsté, J. S. S., Hopmans, E. C., and Cohen, A. S.: Northern
 384 Hemisphere Controls on Tropical Southeast African Climate During the Past 60,000 Years,
 385 *Science*, 322, 252, 2008.

386 Timmermann, A., Lorenz, S. J., An, S. I., Clement, A., and Xie, S. P.: The Effect of Orbital Forcing on
 387 the Mean Climate and Variability of the Tropical Pacific, *J Climate*, 20, 4147-4159,
 388 10.1175/JCLI4240.1, 2007.

389 Truc, L., Chevalier, M., Favier, C., Cheddadi, R., Meadows, M. E., Scott, L., Carr, A. S., Smith, G. F.,
 390 and Chase, B. M.: Quantification of climate change for the last 20,000years from
 391 Wonderkrater, South Africa: Implications for the long-term dynamics of the Intertropical
 392 Convergence Zone, *Palaeogeography, Palaeoclimatology, Palaeoecology*, 386, 575-587,
 393 2013.

394 Tudhope, A. W., Chilcott, C. P., McCulloch, M. T., Cook, E. R., Chappell, J., Ellam, R. M., Lea, D. W.,
 395 Lough, J. M., and Shimmield, G. B.: Variability in the El Niño-Southern Oscillation Through
 396 a Glacial-Interglacial Cycle, *Science*, 291, 1511, 2001.

397 Turner, J. V.: Kinetic fractionation of carbon-13 during calcium carbonate precipitation, *Geochim*
 398 *Cosmochim Ac*, 46, 1183-1191, [http://dx.doi.org/10.1016/0016-7037\(82\)90004-7](http://dx.doi.org/10.1016/0016-7037(82)90004-7), 1982.

399 Vecchi, G. A., and Soden, B. J.: Global Warming and the Weakening of the Tropical Circulation, *J*
 400 *Climate*, 20, 4316-4340, 10.1175/JCLI4258.1, 2007.

401 Venzke, S., Latif, M., and Villwock, A.: The Coupled GCM ECHO-2, *J Climate*, 13, 1371-1383,
 402 10.1175/1520-0442(2000)013<1371:TCGE>2.0.CO;2, 2000.

403 Verschuren, D., Sinninghe Damste, J. S., Moernaut, J., Kristen, I., Blaauw, M., Fagot, M., and Haug,
 404 G. H.: Half-precessional dynamics of monsoon rainfall near the East African Equator,
 405 *Nature*, 462, 637-641, 2009

406 Voarintsoa, N.R.G., Wang, L., Bruce Railsback, L., Brook, G.A., Liang, F., Cheng, H., Lawrence
 407 Edwards, R.: Multiple proxy analyses of a U/Th-dated stalagmite to reconstruct
 408 paleoenvironmental changes in northwestern Madagascar between 370 CE and 1300 CE.
 409 *Palaeogeography, Palaeoclimatology, Palaeoecology* 469, 138-155, 2017.

410 Wang, L.: Late Quaternary paleoenvironmental changes in Southern Africa and Madagascar:
 411 evidence from aeolian, fluvial, and cave deposits, Unpub. dissertation. University of
 412 Georgia, Athens, Georgia, 312pp, 2016.

413 Wang, L., Brook, G.A., 2013. Holocene Climate Changes in Northwest Madagascar: Evidence From
 414 a Two-meter-long Stalagmite From the Anjohibe Cave, Meeting Program of the Association
 415 of American Geographers, Published Online. Session 1512: Paleorecords of our Changing
 416 Earth I: Climate History and Human-Environment Interaction in the Old and New World
 417 Tropics, 2013.

418 Webster, P. J., Moore, A. M., Loschnigg, J. P., and Leben, R. R.: Coupled ocean-atmosphere
 419 dynamics in the Indian Ocean during 1997-98, *Nature*, 401, 356-360, 1999.

420 Williamson, D., Jelinowska, A., Kissel, C., Tucholka, P., Gibert, E., Gasse, F., Massault, M., Taieb, M.,
 421 Van Campo, E., and Wieckowski, K.: Mineral-magnetic proxies of erosion/oxidation cycles
 422 in tropical maar-lake sediments (Lake Tritrivakely, Madagascar): paleoenvironmental
 423 implications, *Earth Planet Sc Lett*, 155, 205-219, [http://dx.doi.org/10.1016/S0012-](http://dx.doi.org/10.1016/S0012-821X(97)00217-3)
 424 [821X\(97\)00217-3](http://dx.doi.org/10.1016/S0012-821X(97)00217-3), 1998.

425 Woo, K. S., and Choi, D. W.: Calcitization of aragonite speleothems in limestone caves in Korea:
 426 Diagenetic process in a semiclosed system, in: *Perspectives on Karst Geomorphology,*
 427 *Hydrology, and Geochemistry - A Tribute Volume to Derek C. Ford and William B. White,*
 428 edited by: Harmon, R. S., and Wicks, C. M., Geological Society of America, 2006.

429 Zhang, H., Cai, Y., Tan, L., Qin, S., and An, Z.: Stable isotope composition alteration produced by
 430 the aragonite-to-calcite transformation in speleothems and implications for paleoclimate
 431 reconstructions, *Sediment Geol*, 309, 1-14, 2014.

432 Zheng, W., Braconnot, P., Guilyardi, E., Merkel, U., and Yu, Y.: ENSO at 6ka and 21ka from ocean–
433 atmosphere coupled model simulations, *Clim Dynam*, 30, 745-762, 10.1007/s00382-007-
434 0320-3, 2008.

435 Zheng, X.-T., Xie, S.-P., Du, Y., Liu, L., Huang, G., and Liu, Q.: Indian Ocean Dipole Response to Global
436 Warming in the CMIP5 Multimodel Ensemble, *J Climate*, 26, 6067-6080, 10.1175/JCLI-D-
437 12-00638.1, 2013.

438 Zinke, J., Dullo, W. C., Heiss, G. A., and Eisenhauer, A.: ENSO and Indian Ocean subtropical dipole
439 variability is recorded in a coral record off southwest Madagascar for the period 1659 to
440 1995, *Earth Planet Sc Lett*, 228, 177-194, 10.1016/j.epsl.2004.09.028, 2004.

441